SCIENTIFIC REPORTS

OPEN

SUBJECT AREAS:
ELECTRONIC PROPERTIES AND DEVICES
ELECTROCATALYSIS
POROUS MATERIALS

Received
25 September 2014

Accepted
22 December 2014

Published
5 June 2015

Correspondence and requests for materials should be addressed to J.F.C. (chenjf@mail.buct.edu.cn) or D.P.C. (caodp@mail.buct.edu.cn)

PAF-derived nitrogen-doped 3D Carbon Materials for Efficient Energy Conversion and Storage

Zhonghua Xiang[1], Dan Wang[1,2], Yuhua Xue[1], Liming Dai[1], Jian-Feng Chen[2] & Dapeng Cao[2]

[1]Centre of Advanced Science and Engineering for Carbon (Case4Carbon), Department of Macromolecular Science and Engineering, Case Western Reserve University, 10900 Euclid Avenue, Cleveland, OH 44106 (USA), [2]State Key Lab of Organic–Inorganic Composites, Beijing University of Chemical Technology, Beijing 100029 (P.R. China).

Owing to the shortage of the traditional fossil fuels caused by fast consumption, it is an urgent task to develop the renewable and clean energy sources. Thus, advanced technologies for both energy conversion (e.g., solar cells and fuel cells) and storage (e.g., supercapacitors and batteries) are being studied extensively. In this work, we use porous aromatic framework (PAF) as precursor to produce nitrogen-doped 3D carbon materials, i.e., N-PAF-Carbon, by exposing NH_3 media. The "graphitic" and "pyridinic" N species, large surface area, and similar pore size as electrolyte ions endow the nitrogen-doped PAF-Carbon with outstanding electronic performance. Our results suggest the N-doping enhance not only the ORR electronic catalysis but also the supercapacitive performance. Actually, the N-PAF-Carbon obtains ~70 mV half-wave potential enhancement and 80% increase as to the limiting current after N doping. Moreover, the N-PAF-Carbon displays free from the CO and methanol crossover effect and better long-term durability compared with the commercial Pt/C benchmark. Moreover, N-PAF-Carbon also possesses large capacitance (385 F g^{-1}) and excellent performance stability without any loss in capacitance after 9000 charge–discharge cycles. These results clearly suggest that PAF-derived N-doped carbon material is promising metal-free ORR catalyst for fuel cells and capacitor electrode materials.

Since the shortage of the traditional fossil fuels and CO_2 emission issues[1,2], it become an urgent task to develop the renewable and clean energy sources. Toward this end, advanced technologies for both energy conversion (e.g., solar cells[3,4] and fuel cells[5]) and storage (e.g., supercapacitors[6] and batteries[7,8]) are being studied extensively. Actually, the catalysts for oxygen reduction play a key role in regulating the performance of fuel cells. However, it is still a great challenge to develop highly efficient and stable oxygen reduction reaction (ORR) electrocatalysts at a low cost since the scarcity, high cost and poor long-term stability of the Pt-based ORR catalysts are main obstacles for commercialization of the fuel cell technology.

The porous carbon family has been demonstrated to be promising candidates for high-performance energy-conversion and storage devices[9]. Recently, N-doping has been widely considered as one of the most feasible approaches to modulate the electronic and catalytic properties of graphene and its derivatives[5,9–16]. A large variety of heteroatom-doped carbon materials, including vertically-aligned nitrogen-containing carbon nanotubes (VA-NCNTs)[12], N-doped graphene[17], nitrogen carbide, and N-doped ordered mesoporous graphitic arrays[18], have been demonstrated to be efficient metal-free ORR electrocatalysts free from CO "poisoning" with a comparable even higher electrocatalytic activity and better long-term operation stability than the commercially available Pt-based electrodes (*e.g.*, C2-20, 20% platinum on Vulcan XC-72R; E-TEK) in alkaline electrolytes. Moreover, N-doping technology has also been extensively used in highly efficient supercapacitors[5,9,10,19,20].

Recently, porous covalent organic materials (COMs)[21–28] with high porosity and controllable structural characteristics as well as multi-chemical functionality have been considered as self-sacrificed precursor to fabricate novel nanoporous carbons including graphene analogues. The COM-derived porous carbons show a lot of advantages. For example, their inherent optimized pore size allows ion migration, and high surface area provides the possibility of formation of an electrostatic charge-separation layer, and a highly ordered structure enables the formation of conductive paths. All these characteristics suggest that COM-derived porous carbon is a class of promising electrocatalyst materials. Pachfule *et al.* employed N-rich porous-organic-frameworks as template to prepare porous nitrogen-rich carbon under 1000°C and obtained ~40 mV enhancement in the onset potential compared to that of a commercial Pt/C catalyst[29]. Zhuang *et al.* prepared the S-/N-doped 2D porous carbons by

the combination of graphene with 2D conjugated microporous polymers as metal-free catalysts for ORR and as supercapacitors[30]. Kou *et al.* synthesized a Aza-fused p-conjugated microporous framework (Aza-CMP) via phenazing ring fusion reaction and Aza-CMP@450 shows large capacitance of ~530 F g^{-1} at 0.2 A g^{-1} [31].

3D structures provide an ideal platform towards the maximization of high specific surface areas, strong mechanical strengths and fast mass and electron transport kinetics for the development of high-performance catalysts, electromechanical and electrochemical devices[10,32]. Actually, the composition and structure of COM materials would determine the electrochemical properties of the resulting porous carbons. Here, to synthesize 3D carbon and reduce the effects of other elements in COM materials, we select porous aromatic framework (PAF-1, in which there are only C and H elements)[33,34] with *dia* topology and ultrahigh BET surface area of 5640 m^2 g^{-1} as self-sacrificed precursor to fabricate high efficient PAF-derived N-doped 3D carbon materials (marked as N-PAF-Carbon) under NH_3 media, and further investigate the electrochemical properties of the N-PAF-Carbon.

Results

Material characterizations. The FT-IR (Figure S1) and solid-state ^{13}C/MAS NMR (Figure S2) measurements reveal the success of C-C coupling in synthesis processes, which is consistent with the previous report[33]. The pore size distribution derived from the N_2 adsorption at 77 K shows that the pore size of as-synthesized PAF-1 is ~1.27 nm (Figure 1b), which also consists with the reported one[35]. Our thermo gravimetric (TG) results suggest the carbonization should be carried out with two steps, i.e., first preheated at 350°C for a period of time and subsequently carbonized at a given high temperature. As shown in Figure 1c, the sample heated directly under N_2 atmosphere without preheating at 350°C almost loss all the weight before 900°C, while the sample with preheating at 350°C for 2 hours can reserve up 70% weight even under 900°C. The 1.54 wt% weight (the inset in Figure 1c) during this process can be ascribed to the adsorbed guests (e.g. O_2, CO_2) in the air due to ultrahigh surface area and the as-synthesized PAF-1 sample can be almost burned with the only adsorbed O_2 molecules in the air.

For comparison, we also prepared undoped 3D PAF derived carbon material. For simplicity, we marked the carbonized PAF carbon materials as PAF-Carbon-T (T= 600, 800 and 1000°C and T is omitted when T = 800°C). As shown in Figure 2a, the sample PAF-Carbon-800 show the best graphitization degree (I_G/I_D=1.07, Figure 2a) among the three PAF-derived carbon samples. The intensity of D band becomes higher than that of G band when the temperature is increased to 1000°C, suggesting the structure of PAF-1 may be completely destroyed and the disordered carbons dominate under 1000°C. The powder X-ray diffraction (XRD) spectra with two pronounced (0 0 2) graphitic peaks at 26° and (1 0 0) at 43° (Figure S3), indicate the formation of graphitic structures during carbonization. Combining the above results with the following ORR activities (*vide infra*), we employed 800°C as the optimal carbonization temperature for preparing N-PAF-Carbon. The Raman results of N-PAF-Carbon show a high ratio of I_G/I_D (1.23, Figure 2a), suggesting good graphitization degree. The X-ray photoelectron spectro-scopic (XPS) measurements show that the atomic percentage of N in N-PAF-Carbon reaches 4.1% (Figure 2b). The XPS N 1s spectra of N-PAF-Carbon (Figure 2c) could be deconvoluted into three sub-peaks: "graphitic" N at 401.1 eV, "pyrrolic" N at 400.1 eV and "pyridinic" N at 398.6 eV, in which the "graphitic" and "pyridinic" N dominate (Figure 2d). Transmission electron microscopic (TEM) images show porous texture in N-PAF-Carbon (Figure 2e). The XRD spectra of N-PAF-Carbon also shows two pronounced (0 0 2) graphitic peaks at 26° and (1 0 0) at 43° (Figure S3), suggesting that the N-PAF-Carbon has good crystalline quality.

Oxygen reduction reaction (ORR) evaluation. The electrocatalytic activities of the non- and N-doped PAF derived carbon materials were explored through cyclic voltammetry (CV), rotating disk

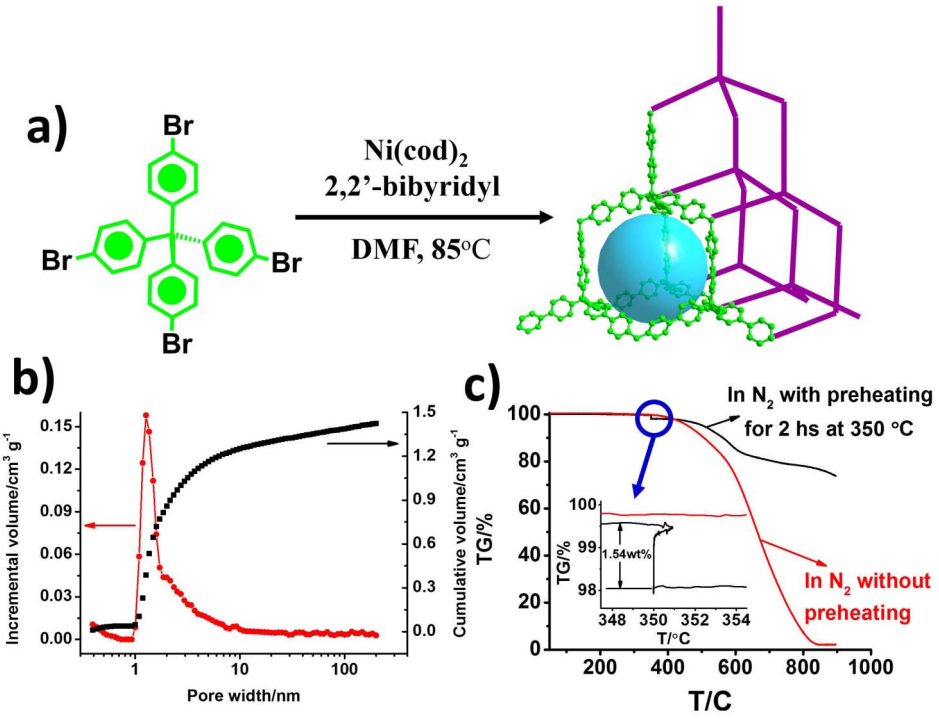

Figure 1 | (a) The scheme for synthesis of PAF-1 materials. The cyan sphere in the right structure refers to the pore in PAF-1 and the purple lines refer to the framework of diamond structure. The actual structures of the statistical PAF-1 materials will be more complex than the one represented. (b) Pore size distribution and cumulative pore volume of PAF-1 obtained by non-local density functional theory modelling on the N_2 adsorption curve. (b) TG analysis of as synthesized PAF-1. The inset refers to the enlargement of the TG analysis in blue circle region.

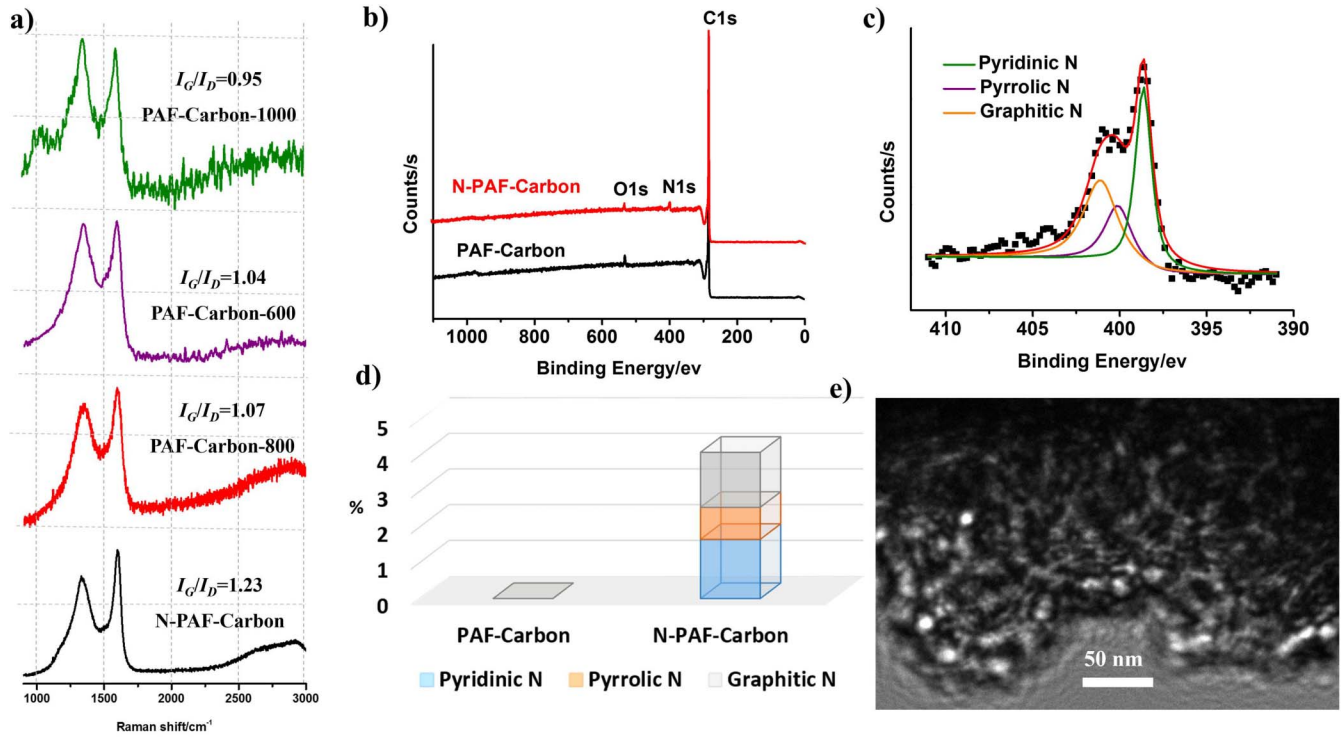

Figure 2 | (a) Raman spectra of PAF-Carbons under different temperature and N-PAF-Carbon. (b) and (c) XPS survey spectrum and high-resolution N 1s spectrum of N-PAF-Carbon. The presence of oxygen can be ascribed to atmospheric O_2, H_2O, or CO_2 adsorbed onto the surface of samples. (d) The percent content of three types of nitrogen in N-PAF-Carbon and PAF-Carbon. (e) TEM images for N-PAF-Carbon.

electrode (RDE), rotating ring disk electrode (RRDE), and chronoamperometric measurements in 0.1 M KOH aqueous solution. Pt/C was also measured for comparation. The RDE measurements show the optimized annealing temperature is to be 800°C since the sample PAF-Carbon-800 possess the highest positive onset and half-wave potential (Figure 3b). Therefore, combining with the above characterization (*vide supra*), we employ 800°C as the carbonization temperature to obtain N-PAF-Carbon. As shown as in Figure 3a, both PAF-Carbon and N-PAF-Carbon show a well-defined cathodic peak centered in the CV curve when the electrolyte was saturated with O_2-saturated 0.1 M KOH, and present a featureless slope for the cathodic current with N_2-saturated 0.1 M KOH within the entire potential range (Figure S4a and S5a). N-PAF-Carbon possesses ~20 mV positive cathodic peak than that of PAF-Carbon, suggesting a more pronounced catalytic activity of N-PAF-Carbon compared with non-doped PAF carbon.

To gain further insight into the ORR process of PAF-Carbon and N-PAF-Carbon, RDE measurements were performed in O_2-saturated 0.1 M KOH electrolyte at a scan rate of 5 mV s^{-1}. As can be seen in Figure 3b, the N-doped sample exhibits much better catalytic activity compared with the non-doped PAF-Carbon. N-PAF-Carbon obtains ~70 mV enhancement for the half-wave potential compared with PAF-Carbon (0.75 vs. 0.68 V) and the limiting current is also improved as much as 80% (from 2.39 mA cm^{-2} to 4.30 mA cm^{-2}) after nitrogen doping. In particular, the N-doped PAF sample shows only 44 mV less for the half-wave potential than the commercial Pt/C. Subsequently, RRDE measurements were carried out to determine their catalytic reaction pathway (Figure 4c). On the basis of the ring and disk currents, the electron transfer number (n) of N-PAF-Carbon was calculated to be 3.50–3.55 at 0 to 0.8 V (vs. reversible hydrogen electrode: RHE), suggesting a mainly four-electron oxygen reduction process. These results consist with those derived from RDE with K-L equation (Figures S5 and S6). In contrast, the electron transfer number for PAF-Carbon was less than 3 under similar condition. Particularly, the peroxide percentage for N-PAF-Carbon was remarkably reduced to <30% from 80% of non-doped PAF-Carbon sample. Basing on the above result, we can infer that the N-doping remarkably enhances the electrocatalystic activity of the PAF-Carbon for ORR. Furthermore, the chronoamperometric measurements show the N-PAF-Carbon is almost free from the CO and methanol crossover effects and holds better long-term durability compared with the commercial Pt/C. These results indicate that N-PAF-Carbon material is promising metal-free ORR electrocatalyst for fuel cells.

Supercapacitance performance. Apart from enhancement for ORR activity of the N-doped technique, we also investigated the effect of N-doping on the supercapacitive behavior. As shown in Figure 4a and 4c, one significant feature in the *I–V* profiles is that no redox peaks are observable, which indicates that PAF derived carbon do not involve redox-related faradic processes during the charge-discharge processes. The *I–V* curves of both PAF-Carbon and N-PAF-Carbon at the different scan rates retain good symmetry, which confirms good electrochemical stability and capacitance. The current of the N-PAF-Carbon is more than 40% larger than those of non-doped PAF-Carbon. The specific capacitance was evaluated from the discharge curves (Figure. 4b and 4d). Under higher current densities than 0.5 A g^{-1}, the capacitances of PAF-Carbon were largely enhanced after N-doping. In particular, the capacitance of PAF-Carbon is increased from 75 to 135 F g^{-1} (with 80% increment) after N-doping at 10 A g^{-1}. When the current density was reduced to 0.2 A g^{-1}, the charge-discharge profiles of PAF-Carbon show remarkable asymmetry character and the hysteresis appears in the discharge process, which may arise from the relatively poor electronic conductivity of PAF-Carbon. In a sharp contrast, the charge-discharge curves of N-PAF-Carbon sample exhibits good symmetry under low current density, even at 0.2 A g^{-1}, which confirms the electronic conductivity of N-PAF-Carbon is largely enhanced after N-doping. The hysteresis results in the 'inflated' supercapacitance of PAF-Carbon (Figure 4c) compared with that

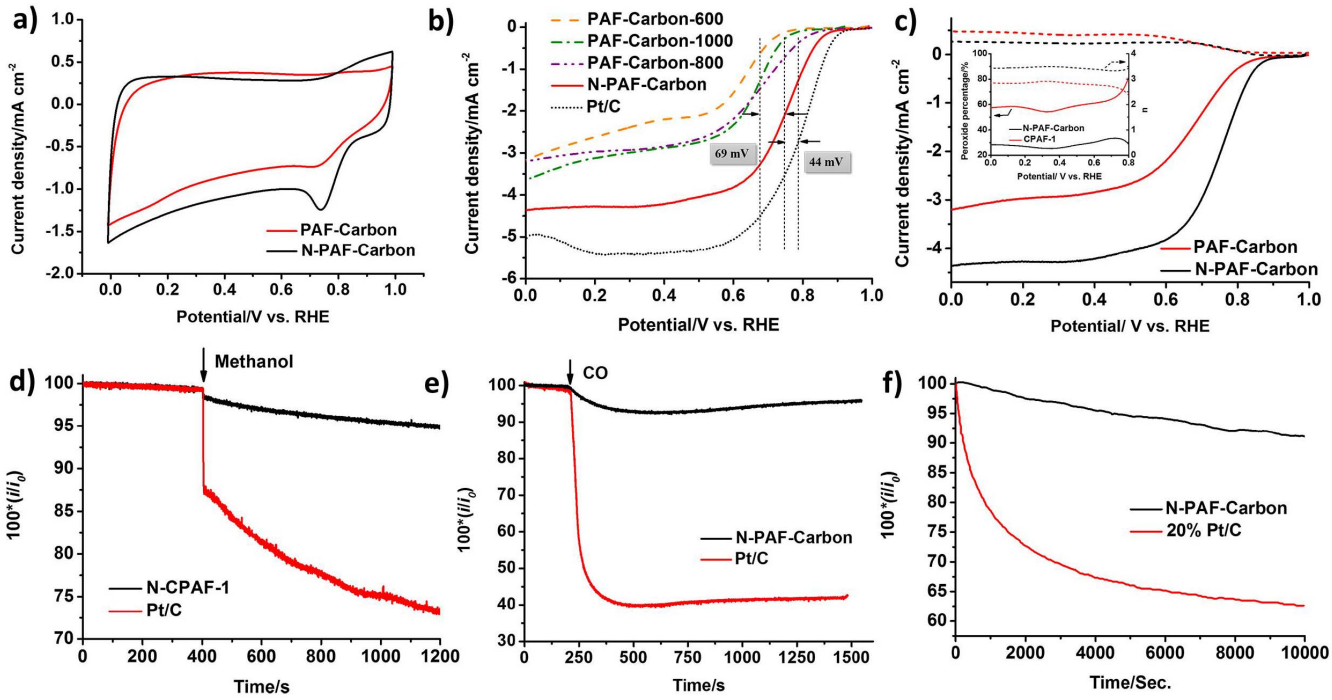

Figure 3 | (a) CV curves of PAF-Carbon and N-PAF-Carbon in O_2-saturated 0.1 M KOH at a sweep rate of 50 mV s^{-1}. (b) LSV curves for PAF-Carbon-600, PAF-Carbon-800, PAF-Carbon-1000, N-PAF-Carbon and Pt/C in O_2-saturated 0.1 M KOH at 1600 rpm at a sweep rate of 5 mV s^{-1}. (c) RRDE curves for PAF-Carbon and N-PAF-Carbon at 1600 rpm. The calculated H_2O_2 yield derived from RRDE is also inserted. (d)–(f), Methanol and CO-poison effects and durability evaluation on i-t chronoamperometric responses for ORR at Pt/C (red) and N-PAF-Carbon (black) electrodes. In figure d, the arrow indicates the addition of 3 mL methanol into the O_2-saturated electrochemical cell after about 400 s. In figure e, the addition of 55 mL min^{-1} CO gas into the 550 mL min^{-1} O_2 flow saturated electrochemical cell after about 250 s.

of N-PAF-Carbon. Particularly, the supercapacitance of N-PAF-Carbon at 0.1 A g^{-1} reaches 385 F g^{-1}, which is close to the previously reported 'ultrahigh' supercapacitance of Aza-CMPs (93–549 F g^{-1}),[31] N-doped graphene foam (484 F g^{-1})[19] but superior to the state-of-the-art nanostructured carbon[6,36], e.g., activated carbon materials (<270 F g^{-1})[37–39], N-rich porous carbon materials (50–330 F g^{-1})[6], carbon nanotubes (50–120 F g^{-1})[40], graphene (135 F g^{-1})[41], N-doped graphene film (280 F g^{-1})[42], and carbon fibers (120–370 F g^{-1})[43] and remarkably outperform those carbons derived from metal organic frameworks (MOFs)[44–46]. (See more results in Table S1 in the Supporting Information).

Discussion

To gain insight into the kinetic behavior of N-doping enhancement for supercapacitance, we further carried out electrochemical impedance spectroscopic (EIS) measurements. In Figure 5a, N-PAF-Carbon exhibits an approximately vertical line, which suggests that N-PAF-Carbon possesses lower diffusive resistivity for the electrolyte ions within the pores. N-PAF-Carbon show a near vertical line that was almost parallel to the Z″ axis (imaginary impedance axis), which indicated ideal capacitive behavior. The impedance spectra are fitted by using the electrical equivalent circuit illustrated in the insert of Figure 5a. In this circuit, R_s is the combined resistance of ionic resistance of electrolyte, intrinsic resistance of substrate and contact resistance at the active material/current collector interface. R_{ct} is the contact interface resistance due to adsorption/desorption of ions on electrode materials. Zw is the Warburg impedance. CPE represents constant phase elements which are substituted for the capacitors to fit the high-frequency capacitive loop and Q is the limit capacitance. All fitted results are shown in Table S2. As shown in Table 1, the R_{ct} was reduced from 1.02 to 0.20 Ω (81.6% decrease). The sum of R_s and R_{ct} is the main contributor to equivalent series resistance (ESR), limiting the specific power of supercapacitors. The PAF derived carbon exhibits 52% shortage of the ESR (0.96 vs. 2.00 Ω) after N-doping. Moreover, we also evaluate the quantitative frequency response by plotting of imaginary capacitance versus frequency derived from the EIS profiles the quantitative. The maximum point of the resultant convex curves represents the frequency f_0, at which purely resistive behavior is transformed into purely capacitive behavior. The reciprocal of f_0 provides a time constant t_0 (Figure 5b, inset), which is a quantitative measure of how fast the device can be reversibly charged and discharged. N-PAF-Carbon possesses much shorter reversible charge-discharge time (4 vs. 7s). All these results show the residence of N-PAF-carbon can be reduced and the electrolyte ions can be moved with faster way within in pores and the charge-discharge process can be finished in a shorter time, compared to PAF-Carbon without N-doping.

The structure effects also co-operatively contribute to the superior capacitive performance of N-PAF-Carbon. First, the "graphitic" and "pyridinic" N species in N-PAF-Carbon increase the density of the electrolyte ions accumulated on the pore walls through electrostatic interactions with protons[31] and facilitate the formation of charge layers. Second, a large surface area is necessary to provide an interface for the formation of electrostatic charge-separation layers in the pores. N-PAF-Carbon possesses a larger specific surface area (SSA) (764 vs. 418 m^2 g^{-1} for S_{BET}, see Figure 5c and Table 1) compared to PAF-Carbon. Moreover, the pore size has a significant effect on the performance of N-PAF-Carbon. pore size is perfectly adapted to the ion size, and ion adsorption is achieved in the most efficient way, by minimizing the free space available[47]. It appears a smaller pore 1.09 nm in N-PAF-Carbon (Figure 5d), which is much closer to the size of electrolyte ions (sulfuric acid electrolyte (proton): 0.42 nm, sulfate: 0.53 nm) than 1.29 nm of PAF-Carbon. At this point, more suitable pore size in N-PAF-Carbon improves the movement of ion species, compared to PAF-Carbon. All these characters indicate that N-PAF-Carbon has outstanding supercapacitive performance.

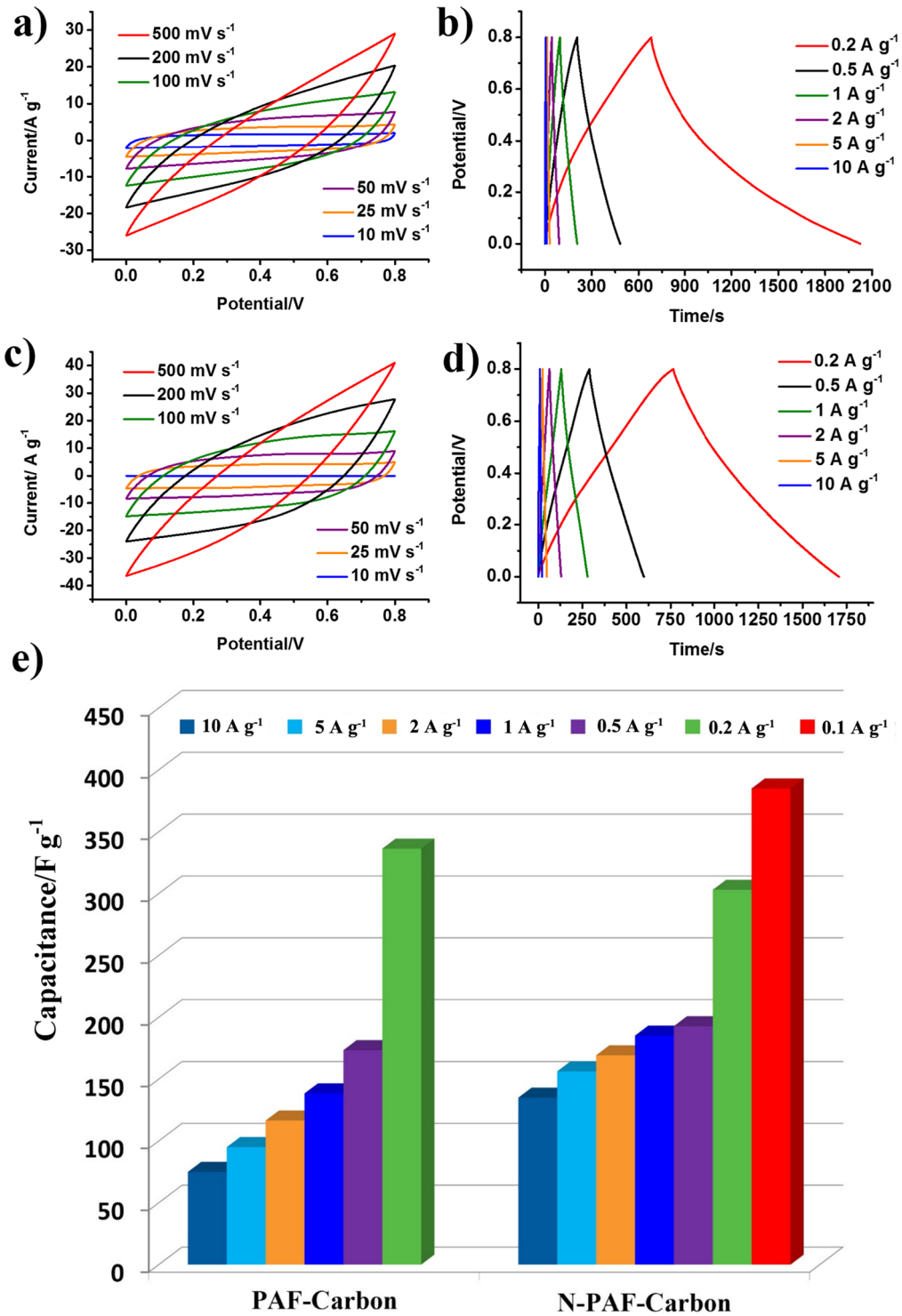

Figure 4 | (a) and (c) CV curves for PAF-Carbon and N-PAF-Carbon at scan rates of 10, 25, 50, 100, 200 and 500 mV s^{-1}. (b) and (d), Charge–discharge profiles for PAF-Carbon and N-PAF-Carbon at current densities of 10, 5, 2, 1, 0.5, and 0.2 A g^{-1}, respectively. (e), Specific capacitance of PAF-Carbon and N-PAF-Carbon at different current densities.

Furthermore, N-PAF-Carbon also exhibits excellent stability without any loss in capacitance after 9000 charge–discharge cycles at a current density of 5 A g^{-1} and the charge–discharge profiles retain the linearity and symmetry well (Figures 5e and 5f). In short, N-PAF-Carbon possesses not only large capacitance but also an excellent cycle life, and is very promising capacitor electrode materials.

In summary, we firstly developed the physical exposure to nitrogen-containing moieties doping approach to introduce N heteroatom into covalent organic materials. Our results suggest the N-doping technique enhance not only the ORR electronic catalysis but also supercapacitive behavior. The N-doped PAF derived carbon obtains ~70 mV enhancement as to half-wave potential and 80% increase as to the limiting current for ORR catalysis. Moreover, the N-doped PAF derived carbon displays free from the CO and methanol crossover effect and better long-term durability compared with the commercial Pt/C benchmark. Furthermore, N-PAF-Carbon based capacitor device is only 0.96 Ω equivalent series resistance

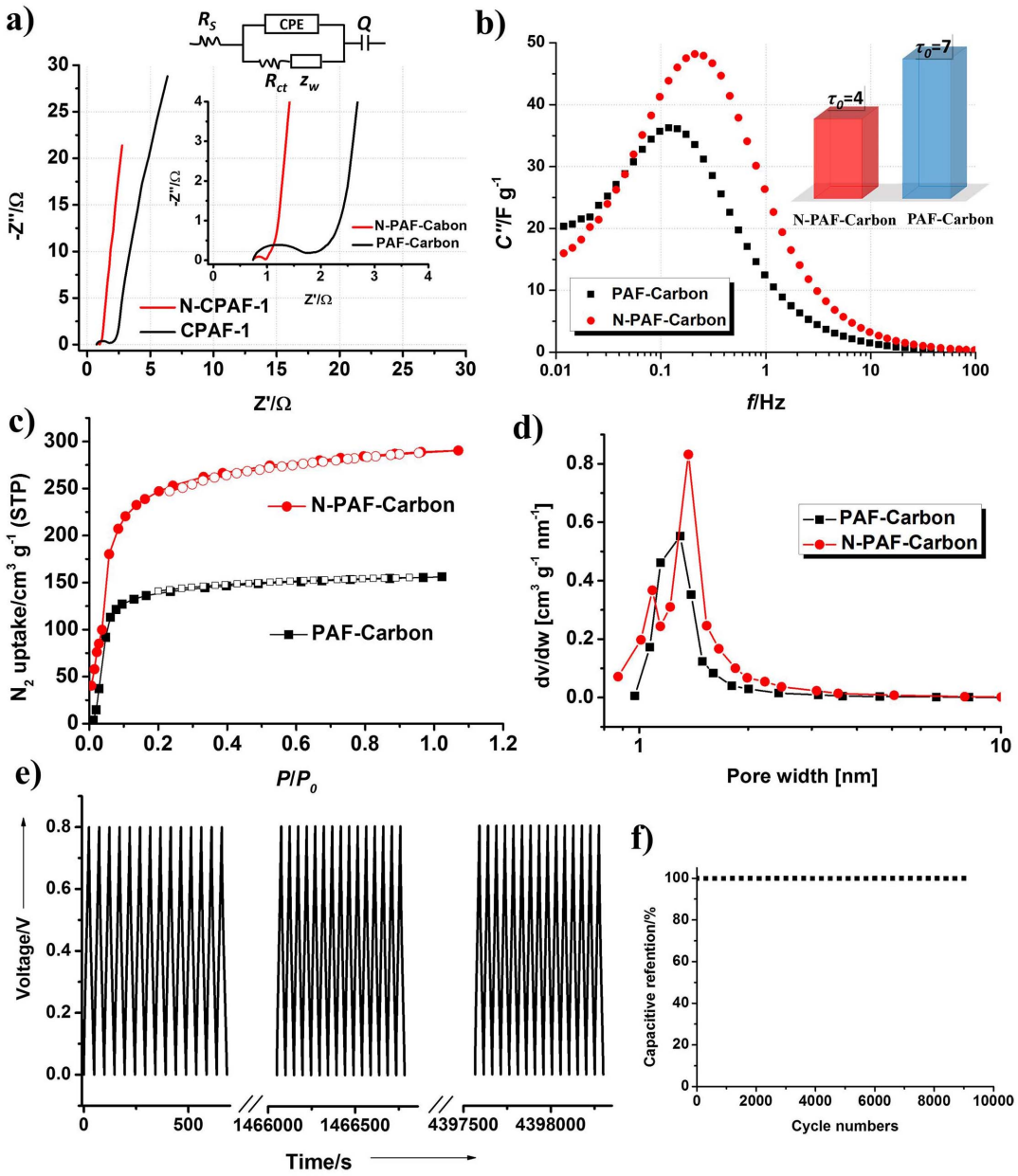

Figure 5 | (a) Nyquist plots of PAF-Carbon and N-PAF-Carbon. Inset shows the impedance in the high and medium-frequency regions and an equivalent circuit as electrode materials is also inserted. (b) Plot of imaginary capacitance versus frequency. The inset shows a plot of the time constant τ_0 of PAF-Carbon and N-PAF-Carbon. (c) N_2 adsorption isotherms of PAF-Carbon and N-PAF-Carbon at 77K. Solid and open symbols represent adsorption and desorption, respectively. (d) NLDFT pore size distributions of PAF-Carbon and N-PAF-Carbon by incremental pore volume. (e) Charge–discharge curves of N-PAF-Carbon during a test of 9000 cycles. The profiles of three time zones of the initial, middle, and last 700 seconds are selected to confirm that they are identical to each other in shape and symmetry. (f) Capacitance percentage of N-PAF-Carbon for a 9000-cycle charge–discharge test at a current density of 5 A g^{-1}.

Table 1 | Summary of porosities, and supercapacitive behaviour of PAF-Carbon and N-PAF-Carbon

Materials	BET SSA[a] [m^2 g^{-1}]	Langmuir SSA [m^2 g^{-1}]	Pore volume[b] [cm^3 g^{-1}]	Pore size distribution[nm]	Capacitance [F g^{-1}]	R_s [Ω]	R_{ct} [Ω]	$R_s + R_{ct}$ [Ω]
PAF-Carbon	418	665	0.24	1.29	336[c]	0.98	1.02	2.00
N-PAF-Carbon	764	1246	0.45	1.37;1.09	385[d]	0.76	0.20	0.96

[a]BET specific surface area (SSA) calculated in the region of P/P_0 = 0.05 to 0.3.
[b]Determined at P/P_0 = 0.9997. The pore volume in this work refers to the total pore volume including the surface condensation.
[c]The capacitance at 0.2 A g^{-1}.
[d]The capacitance at 0.1 A g^{-1}.

low diffusive resistivity of the electrolyte ions within the pores and N-PAF-Carbon possesses not only large capacitance (385 F g^{-1}) but also an excellent performance stability without any loss in capacitance after 9000 charge–discharge cycles. These results clearly indicate that N-PAF-Carbon material is promising metal-free ORR catalyst for fuel cells and promising capacitor electrode materials.

Methods

PAF-1 was prepared according with the previous reported method[33]. By heating the bis(1,5-cyclooctadiene) nickel(0) ([Ni(cod)$_2$] and 2,2′-bipyridyl in dehydrated DMF with Tetrakis(4-bromophenyl)methane at 85°C for overnight, we obtained the PAF-1 powder after drying in vacuum. The scheme for synthesis of PAF-1 was shown in Figure 1a. The activated PAF-1 sample was put into the temperature programming-furnace for degassing at 350°C for 3 hours and then carbonized at a given temperature. The resulting sample was marked as PAF-Carbon. To prepare nitrogen doped 3D carbons (marked as N-PAF-Carbon), we employ the above similar carbonization method, i.e., the activated PAF-1 was put into the temperature programming-furnace for degassing at 350°C for 3 hours and then further carbonized under NH_3 media at a given temperature to produce the final products. The detailed synthetic methods can be found in the supporting information.

1. Figueroa, J. D., Fout, T., Plasynski, S., McIlvried, H. & Srivastava, R. D. Advances in CO_2 capture technology—The U.S. department of energy's carbon sequestration program. *Int. J. Green. Gas Cont.* **2**, 9–20 (2008).
2. Xiang, Z. H., Cao, D. P., Lan, J. H., Wang, W. C. & Broom, D. P. Multiscale simulation and modelling of adsorptive processes for energy gas storage and carbon dioxide capture in porous coordination frameworks. *Energy Environ. Sci.* **3**, 1469–1487 (2010).
3. O'Regan, B. & Gratzel, M. A low-cost, high-efficiency solar cell based on dye-sensitized colloidal TiO_2 films. *Nature* **353**, 734–740 (1991).
4. Xue, Y. *et al.* Nitrogen-Doped Graphene Foams as Metal-Free Counter Electrodes in High-Performance Dye-Sensitized Solar Cells. *Angew. Chem. Int. Ed.* **51**, 12124–12127 (2012).
5. Dai, L., Chang, D. W., Baek, J.-B. & Lu, W. Carbon Nanomaterials for Advanced Energy Conversion and Storage. *Small* **8**, 1130–1166 (2012).
6. Zhang, J. & Zhao, X. S. On the Configuration of Supercapacitors for Maximizing Electrochemical Performance. *ChemSusChem* **5**, 818–841 (2012).
7. Ma, C., Shao, X. & Cao, D. Nitorgen-doped graphene nanosheets as anode materials for lithium ion batteries: a first-principles study. *J. Mater. Chem.* **22**, 8911–8915 (2012).
8. Tarascon, J. M. & Armand, M. Issues and challenges facing rechargeable lithium batteries. *Nature* **414**, 359–367 (2001).
9. Dai, L. Functionalization of Graphene for Efficient Energy Conversion and Storage. *Acc. Chem. Res.* **46**, 31–42 (2012).
10. Zhang, J., Zhao, F., Zhang, Z., Chen, N. & Qu, L. Dimension-tailored functional graphene structures for energy conversion and storage. *Nanoscale* **5**, 3112–3126 (2013).
11. Yu, D. & Dai, L. Self-Assembled Graphene/Carbon Nanotube Hybrid Films for Supercapacitors. *J. Phys. Chem. Lett.* **1**, 467–470 (2009).
12. Gong, K. P., Du, F., Xia, Z. H., Durstock, M. & Dai, L. M. Nitrogen-Doped Carbon Nanotube Arrays with High Electrocatalytic Activity for Oxygen Reduction. *Science* **323**, 760–764 (2009).
13. Zhao, L. *et al.* Visualizing Individual Nitrogen Dopants in Monolayer Graphene. *Science* **333**, 999–1003 (2011).
14. Xiang, Z. H. *et al.* Highly-efficient Electrocatalysts for Oxygen Reduction Based on 2D Covalent Organic Polymers Complexed with Non-precious Metals. *Angew. Chem. Int. Ed.* **53**, 2433–2437 (2014).
15. Xiang, Z. H. *et al.* Nitrogen-Doped Holey Graphitic Carbon from 2D Covalent Organic Polymers for Oxygen Reduction. *Adv. Mater.*, **26**, 3315–3320 (2014).
16. Zhang, P. *et al.* ZIF-derived in situ nitrogen-doped porous carbons as efficient metal-free electrocatalysts for oxygen reduction reaction. *Energy Environ. Sci.* **7**, 442–450 (2014).
17. Qu, L., Liu, Y., Baek, J.-B. & Dai, L. Nitrogen-Doped Graphene as Efficient Metal-Free Electrocatalyst for Oxygen Reduction in Fuel Cells. *ACS Nano* **4**, 1321–1326 (2010).
18. Liu, R., Wu, D., Feng, X. & Müllen, K. Nitrogen-Doped Ordered Mesoporous Graphitic Arrays with High Electrocatalytic Activity for Oxygen Reduction. *Angew. Chem. Int. Ed.* **49**, 2565–2569 (2010).
19. Zhao, Y. *et al.* A Versatile, Ultralight, Nitrogen-Doped Graphene Framework. *Angew. Chem. Int. Ed.* **51**, 11371–11375 (2012).
20. Chen, T. & Dai, L. Carbon nanomaterials for high-performance supercapacitors. *Mater. Today* **16**, 272–280 (2013).
21. Xiang, Z. H. & Cao, D. P. Porous covalent-organic materials: synthesis, clean energy application and design. *J. Mater. Chem. A* **1**, 2691–2718 (2013).
22. Colson, J. W. & Dichtel, W. R. Rationally synthesized two-dimensional polymers. *Nat. Chem.* **5**, 453–465 (2013).
23. Feng, X., Ding, X. & Jiang, D. Covalent organic frameworks. *Chem. Soc. Rev.* **41**, 6010–6022 (2012).
24. Vilela, F., Zhang, K. & Antonietti, M. Conjugated porous polymers for energy applications. *Energy Environ. Sci.* **5**, 7819–7832 (2012).
25. Dawson, R., Cooper, A. I. & Adams, D. J. Nanoporous organic polymer networks. *Prog. Poly. Sci.* **37**, 530–563 (2012).
26. Ding, S.-Y. & Wang, W. Covalent organic frameworks (COFs): from design to applications. *Chem. Soc. Rev.* **42**, 548–568 (2013).
27. Xiang, Z. H. & Cao, D. P. Synthesis of Luminescent Covalent-Organic Polymers for Detecting Nitroaromatic Explosives and Small Organic Molecules. *Macromol. Rapid Comm.* **33**, 1184–1190 (2012).
28. Xiang, Z. H. *et al.* Covalent-organic polymers for carbon dioxide capture. *J. Mater. Chem.* **22**, 22663–22669 (2012).
29. Pachfule, P., Dhavale, V. M., Kandambeth, S., Kurungot, S. & Banerjee, R. Porous-organic-framework-templated nitrogen-rich porous carbon as a more proficient electrocatalyst than Pt/C for the electrochemical reduction of oxygen. *Chem. Euro. J.* **19**, 974–980 (2013).
30. Zhuang, X. *et al.* Two-Dimensional Sandwich-Type, Graphene-Based Conjugated Microporous Polymers. *Angew. Chem. Int. Ed.* **52**, 9668–9672 (2013).
31. Kou, Y., Xu, Y., Guo, Z. & Jiang, D. Supercapacitive Energy Storage and Electric Power Supply Using an Aza-Fused π-Conjugated Microporous Framework. *Angew. Chem. Int. Ed.* **50**, 8753–8757 (2011).
32. Li, C. & Shi, G. Three-dimensional graphene architectures. *Nanoscale* **4**, 5549–5563 (2012).
33. Ben, T. *et al.* Targeted synthesis of a porous aromatic framework with high stability and exceptionally high surface area. *Angew. Chem. Int. Ed.* **48**, 9457–9460 (2009).
34. Lan, J., Cao, D. P., Wang, W., Ben, T. & Zhu, G. S. High-Capacity Hydrogen Storage in Porous Aromatic Frameworks with Diamond-like Structure. *J. Phys. Chem. Lett.* **1**, 978–981 (2010).
35. Li, Y. Q., Ben, T., Zhang, B. Y., Fu, Y. & Qiu, S. L. Ultrahigh Gas Storage both at Low and High Pressures in KOH-Activated Carbonized Porous Aromatic Frameworks. *Sci. Rep.* **3**, 2420 (2013).
36. Ben, T. *et al.* Selective adsorption of carbon dioxide by carbonized porous aromatic framework (PAF). *Energy Environ. Sci.* **5**, 8370–8376 (2012).
37. Kötz, R. & Carlen, M. Principles and applications of electrochemical capacitors. *Electrochim. Acta* **45**, 2483–2498 (2000).
38. Burke, A. Ultracapacitors: why, how, and where is the technology. *J. Power Sources* **91**, 37–50 (2000).
39. Raymundo-Piñero, E., Cadek, M. & Béguin, F. Tuning Carbon Materials for Supercapacitors by Direct Pyrolysis of Seaweeds. *Adv. Funct. Mater.* **19**, 1032–1039 (2009).
40. Feng, X. *et al.* Synthesis of Microporous Carbon Nanofibers and Nanotubes from Conjugated Polymer Network and Evaluation in Electrochemical Capacitor. *Adv. Funct. Mater.* **19**, 2125–2129 (2009).
41. Stoller, M. D., Park, S., Zhu, Y., An, J. & Ruoff, R. S. Graphene-Based Ultracapacitors. *Nano Lett.* **8**, 3498–3502 (2008).
42. Sun, L. *et al.* Nitrogen-doped graphene with high nitrogen level via a one-step hydrothermal reaction of graphene oxide with urea for superior capacitive energy storage. *RSC Adv.* **2**, 4498–4506 (2012).
43. Xu, B. *et al.* Highly mesoporous and high surface area carbon: A high capacitance electrode material for EDLCs with various electrolytes. *Electrochem. Comm.* **10**, 795–797 (2008).
44. Liu, B., Shioyama, H., Jiang, H. L., Zhang, X. B. & Xu, Q. Metal-organic framework (MOF) as a template for syntheses of nanoporous carbons as electrode materials for supercapacitor. *Carbon* **48**, 456–463 (2010).
45. Zhang, P., Sun, F., Shen, Z. & Cao, D. P. ZIF-derived porous carbon: a promising supercapacitor electrode material. *J. Mater. Chem. A* **2**, 12873–12880 (2014).
46. Jiang, H.-L. *et al.* From Metal–Organic Framework to Nanoporous Carbon: Toward a Very High Surface Area and Hydrogen Uptake. *J. Am. Chem. Soc.* **133**, 11854–11857 (2011).
47. Largeot, C. *et al.* Relation between the Ion Size and Pore Size for an Electric Double-Layer Capacitor. *J. Am. Chem. Soc.* **130**, 2730–2731 (2008).

Acknowledgments

L.D. thanks the U.S. Air Force Office of Scientific Research, AFOSR (FA9550-12-1-0037) and National Science Foundation NSF (DMR-1106160) for financial support. DC thanks the NSF of China (No. 91334203, 21274011, 21121064), University Scientific Research Funding (ZZ1304) and Outstanding Talents Plans (RC1301) of BUCT for financial support.

Author contributions

Z.X., L.D. and D.C. produced the original idea, designed experiments, analysed the data and wrote the manuscript. D.W. and J.C. analysed the data and revised the manuscript. Y.X. performed XPS and TEM measurement. All authors have reviewed, discussed and approved the results and conclusions of this article.

Additional information

Supplementary information accompanies this paper at http://www.nature.com/scientificreports

Competing financial interests: The authors declare no competing financial interests.

How to cite this article: Xiang, Z. *et al*. PAF-derived nitrogen-doped 3D Carbon Materials for Efficient Energy Conversion and Storage. *Sci. Rep.* **5**, 8307; DOI:10.1038/srep08307 (2015).